Proceedings of the ASME 2022
Summer Heat Transfer Conference
SHTC2022
Conference: July 11-13, 2022

SHTC2022-78001

A REVISIT TO THE FIRST-PRINCIPLES PREDICTION OF INTERFACIAL THERMAL CONDUCTANCE OF LAYERED MATERIALS USING DIFFUSE MISMATCH MODEL

Jixiong He[1], Jun Liu[1,2*]

[1]Department of Mechanical and Aerospace Engineering,
North Carolina State University, Raleigh, NC 27695, USA
[2]Organic and Carbon Electronics Lab (ORaCEL),
North Carolina State University, Raleigh, NC 27695, USA

ABSTRACT

Among various models for estimating interfacial thermal conductance (ITC) across different material interfaces, the diffuse mismatch model (DMM) has been generally evaluated as a reliable approach for material interfaces at high temperatures. The previous works by DMM have indicated the correct order of magnitude of ITC in isotropic material interfaces. However, it cannot accurately reproduce the ITC for low-dimensional anisotropic layered materials that are desired for many potential applications. Also, the inappropriate mode matching process approximation of the phonon dispersion curve tends to overestimate the ITC. In this paper, we revisited and updated the numerical method in our previous work that utilizes a mode-to-mode comparison within the DMM framework to predict ITC with the first-principles accuracy. We employed this model to calculate ITCs between layered materials such as MoS_2 and graphite and metals such as Al, Au, and Cr. We then compared our values with previous literature data from calculations of phonon dispersion curve and experimental data from time-domain thermoreflectance measurements. With a better mode matching algorithm, the updated numerical method can predict the ITCs with improved accuracy. Further analysis also confirmed that counting only the three acoustic modes and neglecting the low-frequency optical modes lead to significant underestimation of the ITC using DMM.

Keywords: Layered Materials, Metals, Diffuse Mismatch Model, Interfacial Thermal Conductance, Phonon Dispersion, First Principles.

1. INTRODUCTION

Thermal transport across materials interface is important for thermal management in the device design. Recently, few-layer graphene [1-4], graphite [5,6], black phosphorus [7-9], and transition metal dichalcogenides (TMDs) [10-13] as low-dimensional layered materials have garnered focus. These materials have unique properties of electronic, optical, mechanical, and thermal properties. They have wide applications in nanoelectronics devices, such as integrated circuits, spintronics, flexible electronics, and optoelectronics [14-24]. These materials have different structural and thermal properties in the cross-plane and basal-plane directions. When metals form interfaces with these materials, advanced thermal management requires the fundamental understanding of the interfacial thermal transport and a reasonable estimation of the interfacial thermal conductance.

With acceptable accuracy, the Diffuse Mismatch Model (DMM) is conducted for predicting the interfacial thermal conductance in isotropic material interfaces. However, previous applications of the DMM failed to reproduce the same accuracy for anisotropic material interfaces because of the inaccurate phonon group velocities. Detailed knowledge of the phonon dispersion relations of the materials is involved in DMM as important inputs [25]. The DMM with accurate dispersion curves yielded results that varied significantly from the Debye approximation [26]. For layered materials such as graphite, the assumption of an isotropic phonon dispersion results in thermal conductance with a high factor of error around 6 [27]. Recently, an updated framework of DMM was proposed with an anisotropic Debye dispersion to predict the interfacial thermal conductance in graphite, Bi_2Te_3, and high-density polyethylene [28]. Following this work, there was another anisotropic model by utilizing a truncated linear dispersion [29]. The interfacial thermal conductance results still showed a large discrepancy in comparison with the experimental results, because of the inaccurate approximations of the group velocity. In 2019, our group published a paper using first-principles density functional

* Corresponding Author Email: jliu38@ncsu.edu

theory to calculate the phonon dispersion and then matching each phonon mode to predict the interfacial thermal conductance, with improved accuracy compared to the previous methods when comparing with experimental data [30].

In this paper, we provided an updated numerical procedure for a more accurate mode-to-mode matching process to calculate the interfacial thermal conductance between layered materials and metals following the DMM framework. Similarly, as in our previous work, we considered the exact full dispersion of the materials without any approximations. Our results are compared with previous anisotropic models and experimental studies. To evaluate the effectiveness of this new framework, we analyzed the Al-MoS_2 interface to obtain temperature-dependent interfacial thermal conductance values, which has a larger error in our previous work. We also confirmed the conclusion from our previous work: it is imperative to use the exact full dispersion relations in the DMM calculations of anisotropic materials [30].

2. MATERIALS AND METHODS

For thermal interfacial conductance involving metals, multiple energy transport channels could exist, for example, the phonon-phonon interaction, phonon-electron interaction, and electron-electron interaction across the interface. Here, we only consider the phonon-phonon coupling across the interface, following the original assumption of the DMM model. We re-calculated the interfacial thermal conductance for four interfaces at different temperatures: Al-graphite, Au-graphite, Cr-graphite, Al-MoS_2. For layered materials MoS_2 and graphite, the interfacial thermal conductance is calculated in the cross-plane direction. We first obtained the phonon dispersions for the materials forming these interfaces using density functional theory using the software Quantum Espresso [31,32]. To calculate the interfacial thermal conductance, we used the DMM framework [26,27]. For a given interface between two materials A and B, the model assumes that all phonons undergo elastic scattering and lose all memory of their previous state. Let us consider a phonon mode in material A is incident on the interface. The probability that the phonon transmits from A to B is given by [26]

$$\alpha_{A\to B}(\omega') = \frac{\Delta K_B \left[\sum |V\cdot\hat{n}|\right]\delta_{\omega,\omega'}}{\Delta K_A \left[\sum |V\cdot\hat{n}|\right]\delta_{\omega,\omega'} + \Delta K_B \left[\sum |V\cdot\hat{n}|\right]\delta_{\omega,\omega'}}, \qquad (1)$$

where ΔK_A and ΔK_B are the volumes of the discretized cells pertaining to the high-resolution Brillouin zones of A and B. The group velocity is given by V, and the frequency is denoted by ω. The unit vector normal to the interface is given by $\hat{n}$. It is important to note here that the Kronecker delta function $\delta_{\omega,\omega'}$ is unity when the frequencies from the two Brillouin zones are equal and are zero otherwise. It is evident that α is purely a function of the frequency. The transmission probability can now be used to find the interfacial thermal conductance, which is given by [26]

$$G = \frac{1}{2(2\pi)^3}\int \frac{1}{k_B T^2}\alpha\times(\hbar\omega)^2 |V\cdot\hat{n}|\times \frac{\exp\left(\frac{\hbar\omega}{k_B T}\right)}{\left[\exp\left(\frac{\hbar\omega}{k_B T}\right)-1\right]^2}\cdot \qquad (2)$$

Since the phonon loses all memory of its initial state, $\alpha_{A\to B} = 1-\alpha_{B\to A}$. The summation is over all phonon modes. In the calculation of Equation (1) and Equation (2), we set the upper limit of the integration to the maximum frequency of materials A and B. If the phonon modes are not excited at a specific temperature T, the contribution to G is negligible due to the Bose-Einstein distribution in Equation (2).

To obtain the correct conductance, we tested different grids for the two Brillouin zones. The choice of the grid depends primarily on the phonon dispersion curves of the respective materials. If the frequency ranges of both A and B are similar, we can select a grid with a similar number of q-points. However, if material A has, for example, a larger frequency range than material B, the number of q-points for A needs to be greater than that for B. Different grids are tested till we obtain $G_{AB} = G_{BA}$ (practically a numerical difference less than 0.5% can be reached) and the thermal conductance in two directions does not increase with a larger number of q-points.

The crucial part of the revisit in this work is updating the process of matching the phonon modes in materials A and B. Previously, the modes are only separated by the interval of frequency, which is determined by the number of q-points. With a larger number of q-points, the interval of frequency will be smaller. In this case, the mode-matching therefore only depends on the interval of frequency. When we calculated the thermal conductance from A to B, the frequency of modes in A, f_A, will be used as the starting point and the algorithm will find modes in B whose frequency is within the range from $f_A - \frac{\Delta f}{2}$ to $f_A + \frac{\Delta f}{2}$, where Δf is the interval of frequency. In this range, there could be several modes in B with different frequencies matching the mode in A. All those modes in B will be used as inputs for the calculation in Equation (1). The thermal conductance G_{AB} from this previous matching process could result in a large difference from G_{BA} and the number of q-pints should be set carefully, which increases the difficulty of deciding the true interfacial thermal conductance in practice. This matching process could potentially provide thermal conductances with larger errors compared to the experimental data if materials A and B have distinct phonon dispersions. In the updated new algorithm, the starting point of searching is also f_A. Firstly, the algorithm finds modes in B within the range from

$f_A - \frac{\Delta f}{2}$ to $f_A + \frac{\Delta f}{2}$ as the previous version did. Then, the frequencies of modes of B in this range are compared with these of A and the absolute frequency difference is calculated as

$$\Delta_{AB} = |f_A - f_B| . \quad (3)$$

Only the mode in B with the minimum Δ_{AB} can be used for further calculations. According to our observation, the new algorithm will significantly decrease the number of pairs of modes in A and B. Although, in some cases, there might be several modes in B having the same least Δ_{AB}, the new algorithm still provides similar results whether we choose all those modes in B or pick only one of them for the further calculation of interfacial thermal conductance. For example, we calculated the thermal conductance between graphite and metal Cr. The one-mode or several-mode matching process with $(\Delta_{AB})_{\min}$ results in the same thermal conductance around 76 MW/(m^{2}K) at 300 K. The data in our previous work is 89 MW/(m^{2}K) due to counting more modes into one matching process [30].

3. RESULTS AND DISCUSSION

To valid the updated algorithm for interfacial thermal conductance, we re-calculated the interfacial thermal conductance of Al-graphite and Au-graphite as a function of temperature as shown in Figure 1. The updated data (blue line) in both figures match the experimental data better than previous results in Harish et al.'s work (Green line) [30]. To quantify the difference, we calculated the root-mean-square error of the relative difference between the experimental data and all models. The error is 15.7% for our new calculation, 67.8% for Hongkun's model, and 222% for Chen's model for Al-graphite interface.

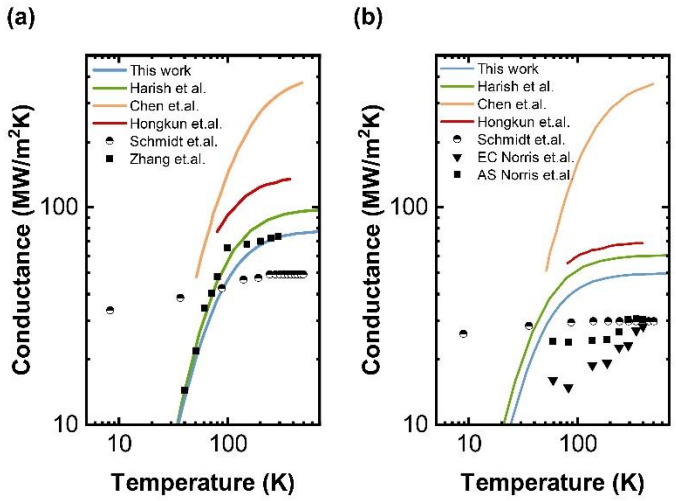

FIGURE 1: Interfacial thermal conductance for (a) Al-graphite and (b) Au-graphite interfaces. The blue lines present our updated results that used the exact full phonon dispersion. The green lines show the old model results by Harish et al. [30] also using the full phonon dispersion. The yellow lines are results taken from Chen's anisotropic DMM [28], and the dark red lines are results taken from Hongkun's anisotropic DMM [29]. The half-moon circles are measured values of conductance by Schmidt et al. [33] using TDTR. The filled squares are measured values by Zhang et al. [34]. For the Au-graphite measurements (b), we also compare the results with electron-cleaved (EC) and As-cleaved (AS) sample results measured by Norris et al. [35] using TDTR.

We also calculated the interfacial thermal conductance between Cr-graphite as shown in Figure 2, which is closer to the experimental data by Schmidt et al. [33] compared to Harish et al.'s work [30].

Finally, we calculated the interfacial thermal conductance between MoS_2-Al and compared the data with previous calculations and experimental data. The experimental data is measured from 100 to 300 K using our time-domain thermoreflectance (TDTR) setup. The experimental details can be found in our previous work [30]. In Figure 3, the updated data (blue line) match our experimental data better than previous results in Harish et al.'s work (Green line) [30]. The updated results also indicate that optical branches have more contributions to interfacial thermal conductance as temperature increases. After updating the mode-matching process, the contributions of acoustic branches to the thermal transport between interface decreases substantially and the contributions from optical branches are larger than expectations compared to the acoustic branches.

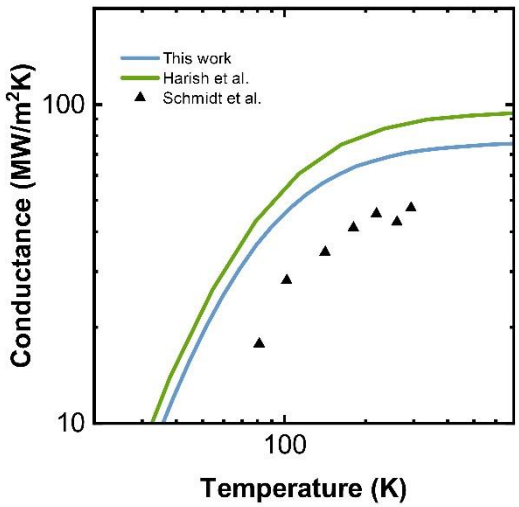

FIGURE 2: Interfacial thermal conductance for the Cr-graphite interface. The blue line is my updated results from Harish et al.'s work [30], green line. The black triangles are measured values of conductance by Schmidt et al. [33] using TDTR.

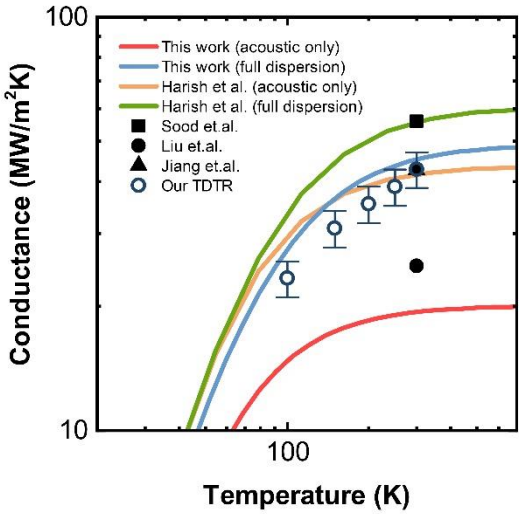

Figure 3: Interfacial thermal conductance for the Al-MoS_2 interface. The red line represents our updated results that considered only acoustic modes, while the blue line represents calculated values using both acoustic and optical modes. The orange line represents old model results by Harish et al. [30] that considered only acoustic modes, and the green line represents calculated values using both acoustic and optical modes. The dark symbols represent experimental results obtained from TDTR measurements at 300 K. The hollow dark blue circles with error bars represent our TDTR measurements at different temperatures.

Based on the discussions above, we believe the updated algorithm can provide more accurate interfacial thermal conductances by the DMM due to an improved mode matching process. The interfacial thermal conductance of Al-graphite, Cr-graphite, Au-graphite, Al-MoS_2, Cr-MoS_2, and Au-MoS_2 are calculated at 300 K by the updated DMM framework and compared with Harish et al.'s work in

Table 1. The new thermal conductance is generally smaller than the previous values because of the optimized matching process in the calculation of transmission probability.

Table 1: The updated thermal conductance compared with previous Harish et al.'s data at 300 K.

Type of interface	Harish et al.'s work (MW/m^2K)	This work (MW/m^2K)
Al-graphite	93	77
Cr-graphite	89	77
Au-graphite	59	50
Al-MoS_2	56	48
Cr-MoS_2	49	39
Au-MoS_2	28	23

4. CONCLUSION

In this paper, we calculated interfacial thermal conductance for Al-graphite, Au-graphite, Cr-graphite, Al-MoS_2, Au-MoS_2, and Cr-MoS_2 interfaces. We found that our updated results agree reasonably better with experimental values than our previous work. The incorporation of exact full dispersion relations without any approximations to the group velocities and accurately matching phonon modes of the two materials is critical to the accuracy of the results. Furthermore, we confirmed that for layered materials, optical phonons have a significant contribution to interfacial thermal conductance. The phonon dispersion for most metals is readily available, which opens the possibility of studying several interfaces between metals and layered materials. As the only inputs for the model are the phonon dispersion relations of the two crystalline materials forming the interface, we can apply this updated model to create a database of interfacial thermal conductance values which can find use in thermal management in several applications, such as optoelectronics, thermoelectric devices, spintronics, and stretchable electronics and nano transistors.

ACKNOWLEDGEMENTS

Computational resources were provided by the High-Performance Computing Center at North Carolina State University and the Extreme Science and Engineering Discovery Environment (XSEDE) which is supported by National Science Foundation grant number ACI-1548562. The authors acknowledge the financial support from the National Science Foundation under the award numbers CBET 1943813 and DMR 2011978.

REFERENCES

[1] M. Uz, K. Jackson, M. S. Donta, J. Jung, M. T. Lentner, J. A. Hondred, J. C. Claussen, and S. K. Mallapragada, Fabrication of high-resolution graphene-based flexible electronics via polymer casting, Scientific reports **9**, 1 (2019).

[2] S.-W. Ng, N. Noor, and Z. Zheng, Graphene-based two-dimensional Janus materials, NPG Asia materials **10**, 217 (2018).

[3] X. Zhang, L. Hou, A. Ciesielski, and P. Samorì, 2D materials beyond graphene for high-performance energy storage applications, Advanced Energy Materials **6**, 1600671 (2016).

[4] Y.-M. Lin, C. Dimitrakopoulos, K. A. Jenkins, D. B. Farmer, H.-Y. Chiu, A. Grill, and P. Avouris, 100-GHz transistors from wafer-scale epitaxial graphene, Sci **327**, 662 (2010).

[5] Y. Kobayashi *et al.*, Growth and optical properties of high-quality monolayer WS2 on graphite, Acs Nano **9**, 4056 (2015).

[6] L. Paulatto, F. Mauri, and M. Lazzeri, Anharmonic properties from a generalized third-order ab initio approach: Theory and applications to graphite and graphene, Phys. Rev. B **87**, 214303 (2013).
[7] B. Sun, X. Gu, Q. Zeng, X. Huang, Y. Yan, Z. Liu, R. Yang, and Y. K. Koh, Temperature dependence of anisotropic thermal-conductivity tensor of bulk black phosphorus, Adv. Mater. **29**, 1603297 (2017).
[8] F. Xia, H. Wang, and Y. Jia, Rediscovering black phosphorus as an anisotropic layered material for optoelectronics and electronics, Nat. Commun. **5**, 1 (2014).
[9] M. Li, J. S. Kang, H. D. Nguyen, H. Wu, T. Aoki, and Y. Hu, Anisotropic thermal boundary resistance across 2D black phosphorus: Experiment and atomistic modeling of interfacial energy transport, Adv. Mater. **31**, 1901021 (2019).
[10] J. D. Caldwell, I. Aharonovich, G. Cassabois, J. H. Edgar, B. Gil, and D. Basov, Photonics with hexagonal boron nitride, Nature Reviews Materials **4**, 552 (2019).
[11] C. Elias *et al.*, Direct band-gap crossover in epitaxial monolayer boron nitride, Nat. Commun. **10**, 1 (2019).
[12] S. Bertolazzi, J. Brivio, and A. Kis, Stretching and breaking of ultrathin MoS2, ACS nano **5**, 9703 (2011).
[13] G. Zhu, J. Liu, Q. Zheng, R. Zhang, D. Li, D. Banerjee, and D. G. Cahill, Tuning thermal conductivity in molybdenum disulfide by electrochemical intercalation, Nat. Commun. **7**, 1 (2016).
[14] K. Esfarjani, G. Chen, and H. T. Stokes, Heat transport in silicon from first-principles calculations, Phys. Rev. B **84**, 085204 (2011).
[15] O. Hellman and I. A. Abrikosov, Temperature-dependent effective third-order interatomic force constants from first principles, Phys. Rev. B **88**, 144301 (2013).
[16] O. Hellman and D. A. Broido, Phonon thermal transport in Bi2Te3 from first principles, Phys. Rev. B **90**, 134309 (2014).
[17] T. Tadano and S. Tsuneyuki, Self-consistent phonon calculations of lattice dynamical properties in cubic SrTiO 3 with first-principles anharmonic force constants, Phys. Rev. B **92**, 054301 (2015).
[18] T. Tadano and S. Tsuneyuki, First-principles lattice dynamics method for strongly anharmonic crystals, J. Phys. Soc. Jpn. **87**, 041015 (2018).
[19] M. Puligheddu, Y. Xia, M. Chan, and G. Galli, Computational prediction of lattice thermal conductivity: A comparison of molecular dynamics and Boltzmann transport approaches, Phys. Rev. Mater. **3**, 085401 (2019).
[20] T. Feng, B. Qiu, and X. Ruan, Coupling between phonon-phonon and phonon-impurity scattering: A critical revisit of the spectral Matthiessen's rule, Phys. Rev. B **92**, 235206 (2015).
[21] D. G. Cahill, W. K. Ford, K. E. Goodson, G. D. Mahan, A. Majumdar, H. J. Maris, R. Merlin, and S. R. Phillpot, Nanoscale thermal transport, J. Appl. Phys. **93**, 793 (2003).
[22] J. Larkin, J. Turney, A. Massicotte, C. Amon, and A. McGaughey, Comparison and evaluation of spectral energy methods for predicting phonon properties, J. Comput. Theor. Nanosci. **11**, 249 (2014).
[23] A. J. McGaughey and J. M. Larkin, Predicting phonon properties from equilibrium molecular dynamics simulations, Annu. Rev. Heat Transfer **17** (2014).
[24] A. S. Henry and G. Chen, Spectral phonon transport properties of silicon based on molecular dynamics simulations and lattice dynamics, J. Comput. Theor. Nanosci. **5**, 141 (2008).
[25] J. C. Duda, T. E. Beechem, J. L. Smoyer, P. M. Norris, and P. E. Hopkins, Role of dispersion on phononic thermal boundary conductance, J. Appl. Phys. **108**, 073515 (2010).
[26] P. Reddy, K. Castelino, and A. Majumdar, Diffuse mismatch model of thermal boundary conductance using exact phonon dispersion, Appl. Phys. Lett. **87**, 211908 (2005).
[27] J. C. Duda, J. L. Smoyer, P. M. Norris, and P. E. Hopkins, Extension of the diffuse mismatch model for thermal boundary conductance between isotropic and anisotropic materials, Appl. Phys. Lett. **95**, 031912 (2009).
[28] Z. Chen, Z. Wei, Y. Chen, and C. Dames, Anisotropic Debye model for the thermal boundary conductance, Phys. Rev. B **87**, 125426 (2013).
[29] H. Li, W. Zheng, and Y. K. Koh, Anisotropic model with truncated linear dispersion for lattice and interfacial thermal transport in layered materials, Phys. Rev. Mater. **2**, 123802 (2018).
[30] H. Subramanyan, K. Kim, T. Lu, J. Zhou, and J. Liu, On the importance of using exact full phonon dispersions for predicting interfacial thermal conductance of layered materials using diffuse mismatch model, Aip Advances **9**, 115116 (2019).
[31] P. Giannozzi *et al.*, QUANTUM ESPRESSO: a modular and open-source software project for quantum simulations of materials, J. Phys.: Condens. Matter **21**, 395502 (2009).
[32] P. Giannozzi *et al.*, Advanced capabilities for materials modelling with Quantum ESPRESSO, J. Phys.: Condens. Matter **29**, 465901 (2017).
[33] A. J. Schmidt, K. C. Collins, A. J. Minnich, and G. Chen, Thermal conductance and phonon transmissivity of metal–graphite interfaces, J. Appl. Phys. **107**, 104907 (2010).
[34] H. Zhang, X. Chen, Y.-D. Jho, and A. J. Minnich, Temperature-Dependent Mean Free Path Spectra of Thermal Phonons Along the c-Axis of Graphite, Nano Lett. **16**, 1643 (2016).
[35] P. M. Norris, J. L. Smoyer, J. C. Duda, and P. E. Hopkins, Prediction and measurement of thermal transport across interfaces between isotropic solids and graphitic materials, J. Heat Transfer **134** (2012).